CrossMark

RESEARCH ARTICLE

Sonochemically synthesized hydroxy-functionalized graphene–MnO$_2$ nanocomposite for supercapacitor applications

Dipanwita Majumdar[1] · Swapan Kumar Bhattacharya[2]

Abstract A simple, facile, cost-effective and reproducible one-pot sonochemical synthesis of hydroxy-functionalized graphene–MnO$_2$ nanocomposite of various compositions is executed starting from pristine graphite powder. Morphology of all the as-synthesized composites has been characterized with scanning electron microscopy and high-resolution transmission electron microscopy. Further, X-ray diffraction, Thermogravimetric analyses, Fourier transform-infrared spectroscopy, and Raman spectroscopy have been employed to understand the existing phases, thermal stability, nature of functionalization, and existing interactions between the components, respectively, in all the nanocomposites studied. The as-synthesized sample (GM2) having molar ratio of C:Mn of 0.931 exhibits an improved and synergistic capacitive behavior. The crystalline MnO$_2$ nanosheets anchored on hydroxy-functionalized graphene (GM2) displayed superior specific capacitance of 376.7 Fg^{-1} as determined by cyclic voltammetry, carried out at a scan rate of 2 mVs^{-1} in the voltage window of -0.2 to $+0.4$ V versus SCE in 1 M Na$_2$SO$_4$ medium. It also displayed appreciable capacity retention ($\sim 90\%$) even after 1000 cycles, observed from galvanostatic charging/discharging measurements. Moreover, electrochemical impedance spectroscopic studies of the GM2 sample substantiate better electrical conductivity and ion transport performances, assuring its potentiality as a promising electrode material for energy storage devices.
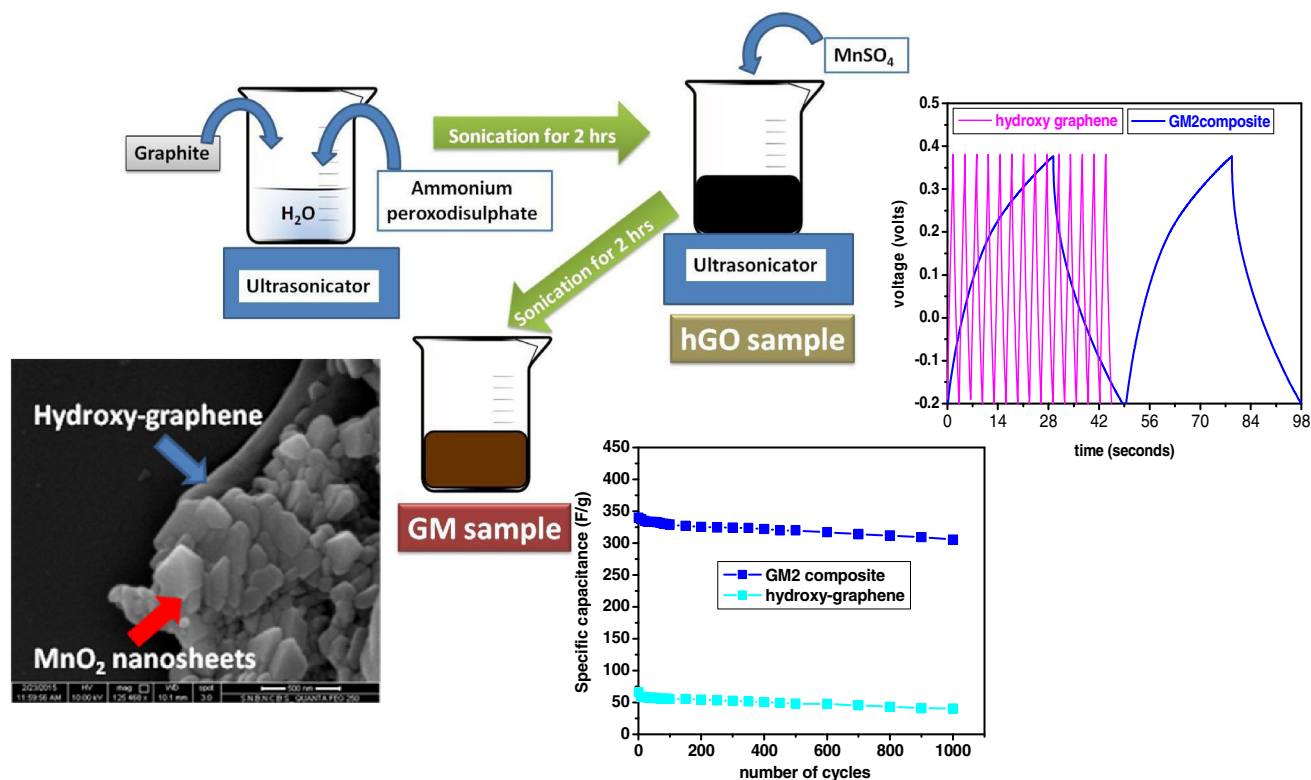
✉ Dipanwita Majumdar
wbesdmajumdar@gmail.com

1   Department of Chemistry, Barasat Government College, Barasat, Kolkata 700124, India

2   Physical Chemistry Section, Department of Chemistry, Jadavpur University, Jadavpur, Kolkata 700032, India

🍦 Springer

Graphical Abstract

Keywords Hydroxy-graphene · Electrochemical performances · Manganese dioxide nanosheets supercapacitance · Nanocomposite

1 Introduction

For the last few years, extensive strategies have been targeted worldwide to develop novel, renewable energy storage devices with higher energy and superior power densities that can be successfully used in vehicles and/or industries with controlled environmental pollution. Highly efficient "Electrochemical capacitors"—popularly known as "Supercapacitors," due to their improved power delivering ability, durability, recyclability, and high charge propagation dynamics, ease of fabrication, have turned out to be one of the most accepted alternatives and challenging field for research community [1–4]. Currently used electrode materials for "supercaps" are largely based on graphene-based materials—particularly the functionalized graphene-metal oxide nanocomposites [5–8]; as they are found to exhibit increased effective surface area, mechanical stability, enhanced electrical conductivity, reversible double-layer charging–discharging behavior, superior and synergistic charge storing capacities [5–9]. Recently, similar experiences have been reported by our group as well [8].

Among the promising metal oxides available, MnO_2, due to its appreciable electrochemical performance, limited environmental toxicity, and lower production cost, has extensive applications in energy storage devices [10–12]. Moreover, it exists as polymorphic system, such as α, β, γ, δ types, offering distinctive properties in aid [13, 14]. Many researchers have explored the influence of size and shape of the MnO_2 nanostructures namely flower-like, sponges, needle-shaped, spherical, rods, wires, nanowalls, as well as a honeycomb-like "opened" structure deposited on the graphene layers to achieve superior electrochemical features [9–12, 15–31]. Some of the relevant works are summarized in Table 1.

The above explorations indicate that larger surface area and greater loading of pseudocapacitive material (MnO_2) are required to obtain better electrochemical responses. So, researchers contemplated exfoliating graphite to graphene oxide containing more oxygen groups which in one hand has an intrinsic pseudocapacitive behavior that will enforce synergic effect in electrochemical performances in the composite besides the ability of holding larger amount of MnO_2 in the layers due to enhanced functionalization [31]. Thus, to further explore the influence of oxygen functionalization on the graphene layers, Yang et al. carried out systematic study with graphene oxides of different extents of oxygen functionalities. They observed that surface area and functionalities of GO have significant effects on the

Table 1 Summary of research works based on functionalized graphene–MnO$_2$ nanocomposites

Composite morphology	Method of synthesis	Specific capacitance and electrochemical parameters	Ref.
Graphene–MnO$_2$ composites	Polymer-assisted chemical reduction	324 Fg^{-1} in the range of 0.0 to +1.0 V at scan rate of 10 mVs^{-1} in 1 M Na$_2$SO$_4$ aqueous solution	[20]
Graphene–MnO$_2$ composites	Microwave irradiation	310 Fg^{-1} in the range of −0.3 to +0.8 V at a scan rate of 2 mVs^{-1} in 1.0 (M) Na$_2$SO$_4$ aqueous solution	[21]
Reduced graphene (HRG)/MnO$_2$ composites	Hydrothermal method	211.5 Fg^{-1} in the range of 0.0 to +1.0 V at a potential scan rate of 2 mVs^{-1} in 1.0 (M) Na$_2$SO$_4$ aqueous solution	[22]
Graphene/MnO$_2$ nanowall hybrids (GMHs)	One-step electrochemical method	122 Fg^{-1} in the range of −0.2 to +1.0 V at higher scan rate of 10 mVs^{-1} in 1 (M) Na$_2$SO$_4$ aqueous solution	[23]
Graphene-decorated-flower-like MnO$_2$ nanostructures	Electro-deposition method	328 Fg^{-1} in the potential ranges of −1.0 to +0.4 V at a charging current of 1 mA, in 0.1 (M) Na$_2$SO$_4$ aqueous solution	[11]
MnO$_2$ nanowire/graphene composite (MGC)	solution phase assembly method	30.1 Fg^{-1} in the potential ranges of 0.0 to +2.0 V at current density of 0.5 Ag^{-1}, in 0.1 (M) Na$_2$SO$_4$ aqueous solution	[25].
Graphene-wrapped honeycomb-like "opened" structure MnO$_2$ nanocomposites	Wet chemical co-assembly method	210 Fg^{-1} in the potential ranges of 0.0–1.0 V at current density of 0.5 Ag^{-1}, in 1.0 (M) Na$_2$SO$_4$ aqueous solution.	[26]
Nanostructured α-MnO$_2$ (SDS)/GO composite	Hydrothermal method	280 Fg^{-1} in the potential ranges of −1.0 to +0.75 V at current density of 0.5 Ag^{-1}, in 1.0 (M) Li$_2$SO$_4$ aqueous solution.	[27]
2D planar-structured δ-MnO$_2$ nanosheets integrated on graphene sheets	Chemical method	267 Fg^{-1} in the potential ranges of −0.70 to +0.70 V at current density of 0.2 Ag^{-1} using gel electrolyte	[9]
Reduced graphene oxide–nanoneedle manganese oxide composites	Chemical method	383 Fg^{-1} in the range of −0.10 to +0.90 V, scan rate of 10 mVs^{-1} in 1.0 (M) Na$_2$SO$_4$ aqueous solution	[28]
Graphene/MnO$_2$	Electro-deposition method	315 Fg^{-1} in the range of 0.0 to +0.85 V, scan rate of 5 mVs^{-1} in 0.5 (M) Na$_2$SO$_4$ aqueous solution	[29]
Freestanding, lightweight three-dimensional (3D) graphene networks, loaded with MnO$_2$	Electro-deposition method	130 Fg^{-1} in the range of 0.0 to +1.0 V using polymer separator, scan rate of 2 mVs^{-1}	[30].
Graphene oxide supported by needle-like MnO$_2$ nanocrystals (GO/MnO$_2$ nanocomposites)	Chemical route	192.7 Fg^{-1} in the range of 0.0 to +1.0 V at 200 mAg^{-1} current density in 1.0 (M) Na$_2$SO$_4$ aqueous solution	[5]
Graphene/MnO$_2$ composite paper	Three-step chemical route	256 Fg^{-1} in the range of 0.0 to +0.8 V at 500 mAg^{-1} current density in 0.1 M Na$_2$SO$_4$ aqueous solution	[12]

morphology and electrochemical activity of MnO$_2$, which led to the higher loading amount of MnO$_2$ on the more functionalized graphene oxide [21, 32]. As a result, the nanocomposites with MnO$_2$ embedded on larger functionalized graphene oxide showed larger capacitance (307.7 F g^{-1}) and better electrochemical activity.

However, exfoliation of the graphene layers led to decrease in the electrical conductivity and increase in the equivalent series resistance (ESR), which in turn will reduce the electrochemical efficiency. Hence, to restore the above achievements as well as increase the electrical conductivity of the samples, several measures have been adopted. One of such instances includes the work reported by Bao group. They developed "conductive wrapping" method to improve the supercapacitor performance of graphene/MnO$_2$-based nanostructured electrodes greatly [29, 33]. However, addition of too many materials may,

often in numerous cases, subdue the intrinsic property of components. Therefore, we have thrusted on optimizing the oxygen content on graphene sheets so that both the features, intrinsic pseudocapacitive behavior of oxygen-functionalized graphene oxide and the ability of holding larger quantity of MnO$_2$ in the layers due to enhanced functionalization, are restored in the composite.

In recent times, we have explored that hydroxy-functionalized graphene (hGO) has great potential applications in developing various nano-devices in the field of electrochemical energy, [34]. Consequently, anchoring of MnO$_2$-nanostructures onto hGO might introduce superior electrochemical features. Different morphologies have resulted due to compositional variations with varying charge storage capabilities. Hence, the main focus of the exploration is to synthesize hydroxy-functionalized graphene/MnO$_2$ (hGO–MnO$_2$) nanocomposites using facile one-pot

sonochemical technique and determine/tune the optimal conditions, where both components synergistically establish superior electrochemical performances.

2 Experimental details

2.1 Synthesis of GM composites

The method of synthesis of GM samples is described in Scheme 1. Graphite powder (Loba, Finely divided) ("X" g) was thoroughly mixed with ammonium peroxodisulfate (APS) $(NH_4)_2S_2O_8$ (5 g) and 200 ml double distilled water was added and sonicated (35 kHz) for 2 h. Then "Y" g of Manganese(II) sulfate monohydrate was added in proportions as summarized in Table 2. The mixture turned dark brown, and the ultrasonication was continued for another 2 h. The resultant mass was centrifuged, repeatedly washed with distilled water and then dried at 90 °C in hot oven. It is worth mentioning that the application of sonochemical energy delivers necessary activation energy for the of MnO_2 particle formation from the oxidation of Mn(II) ions by oxidant ammonium peroxodisulfate ion, which simultaneously also oxidizes individual graphite layers to hydroxy-graphene. Optimum oxidation of graphene sheets with hydroxyl groups provides adequate nucleation sites for the formation of MnO_2 nanosheets which anchor onto the surfaces of functionalized graphene sheets. To ensure the optimized concentration to obtain the best electrochemical performance, we have prepared GM1 and GM3 samples and compared their electrochemical signatures

with GM2 sample. For comparison, hydroxy-graphene (h-GO) sample is synthesized under similar condition without addition of Mn(II) ion. Similarly, Blank-MnO_2 is also prepared under condition without addition of graphite.

2.2 Characterization details of GM2 composite

The as-synthesized powdered samples were characterized using X-ray powder diffraction (XRD, PANalytical X'Pert Pro diffractometer with Cu K radiation ($\lambda = 0.154$ nm)). Fourier transform-infrared spectroscopy (FTIR) spectra were carried out in solid state using KBr pellets in Perkin Elmer Spectrum 100 FTIR Spectrometer. The morphologies of the samples were characterized by field-emission scanning electron microscopy (FESEM, JEOL; Quanta FEG 250 and ZEISS EVO-MA 10 models) and transmission electron microscopy (TEM, JEOL, and TECNAI models). Thermogravimetric analyses (TGA) were carried out in SDT600 under dinitrogen gas atmosphere at a heating rate of 10 °C/min. The electrochemical studies were carried out in three-electrode system using electrode materials deposited on graphite-carbon electrode as working electrode, Pt wire as counter electrode, and saturated calomel electrode (SCE) as reference electrode in 0.1(M) Na_2SO_4 aqueous solution using CH-instrument for electrochemical studies while the charging–discharging was carried out with the same cell system using Autolab PGSTAT30 instrument at ambient temperature (25 °C). The working electrode was prepared as follows. The composites were thoroughly suspended in aqueous solution (1 mg/ml), and 0.01 ml of each suspension was drop-
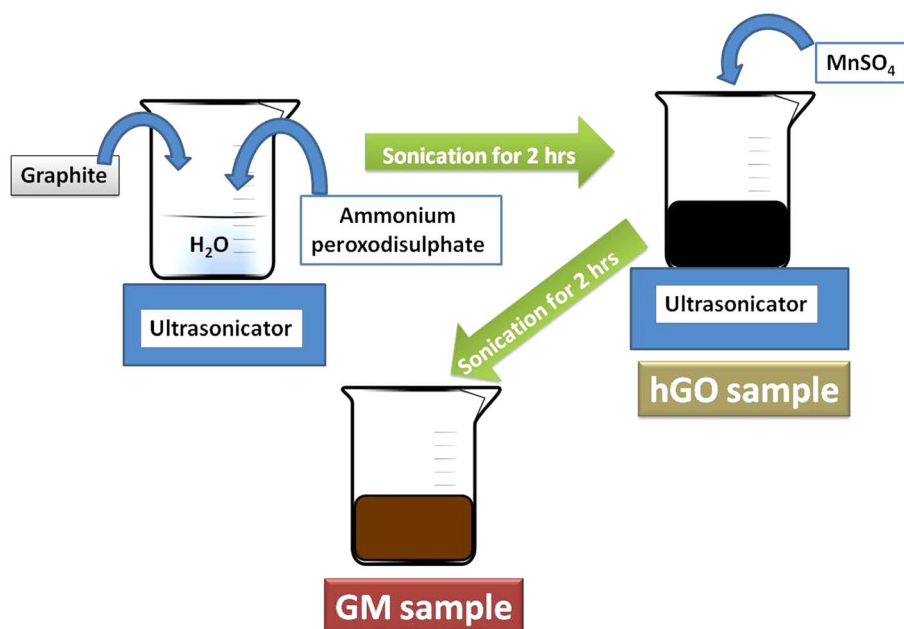
Scheme 1 Diagram representing method of synthesis of GM composite

Table 2 Composition of GM samples

Sample name	Graphite (X) (g)	MnSO₄ (Y) (g)	GRAPHITE:MnSO₄ ratio (w/w) =	C:Mn molar ratio
GM1	0.25	7	0.03	0.140
GM2	1.5	7	0.2	0.931
GM3	0.25	0.25	1	4.654

coated on the graphite-carbon electrode circular surface of diameter 26 mm and dried at 110 °C for 15 min. The results of the characterized samples are discussed below. Raman studies were carried out in solid state using 514 nm laser excitation using MODEL T64000 (Make Jobin Yvon Horiba, France), Argon-Krypton mixed ion gas laser. MODEL 2018 RM (Make Spectra Physics, USA) as excitation source, Optical Microscope MODEL BX41 (Make Olympus, Japan) as collection optic sytem and Thermoelectric cooled front illuminated 1024 256 CCD. MODEL SynpseTM (Make Jobin Yvon Horiba, France) detector. For EIS study, working electrode: GM (70%):-super P carbon (20%):PVDF (10%) casted on nickel (Ni) foil of dimension 1.5 cm × 1.5 cm, reference electrode: Ag/AgCl (3 M KCl), counter electrode: Platinum(Pt)mesh (2 cm × 2 cm), electrolyte: 1.0 M Na₂SO₄ (aqueous solution), in Galvanostat-Potentiostat (PGSTAT302 N, Autolab, The Netherlands). Frequency range of 100 kHz to 0.1 Hz with an AC amplitude of 5 mV and integration time of 0.25 s. BET surface area analyses were carried out in Quantachrome Instruments version 10.01, using dinitrogen gas as adsorbate; sample weight = 0.410 g (GM2 sample), 0.369 g (h-GO sample); and outgassing time: 6 h at 150 °C, respectively.

3 Results and discussion

The phase study of the as-prepared samples was investigated by the x-ray diffraction (XRD) analyses. Figure 1a displays the powdered XRD pattern of the GM2 composite. The main peaks at 18.05°(200), 25.7°(220), 28.9°(310), 37.5°(211), confirm the presence of both α-MnO₂ (black) (JCPDS 44-0141) as well as graphitic carbon phases (blue), although peaks got slightly shifted due to composite formation [15, 35–37]. The inset shows XRD pattern of pristine h-GO sample, as previously reported by our group [34]. The relative low peak intensity at 26.4° (002) in comparison to that of 54.7° in XRD the composite with respect to that in h-GO sample is attributed to the growth of MnO₂ nanosheets in between the hGO sheets in GM2 composite. The XRD pattern of blank-MnO₂ shown in Figs. SI-6a is assigned to reflections of α-MnO₂ phase (JCPDS file no. 44-0141). XRD patterns of GM1 and GM3 samples show peaks having very much resemblance to
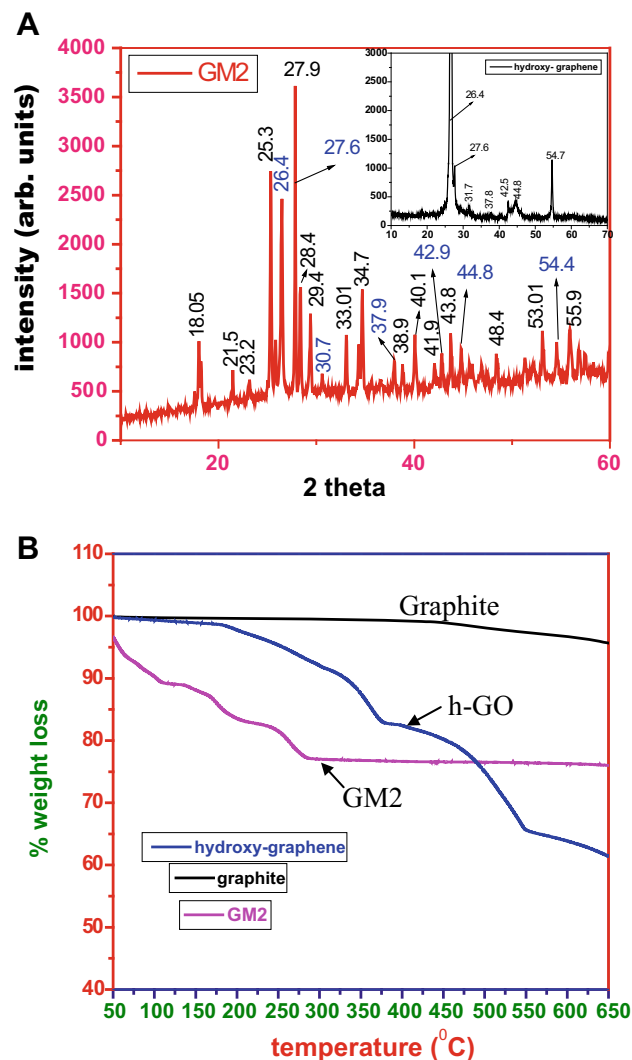

Fig. 1 a XRD pattern of GM2 (*inset*: hydroxy-graphene). b TGA of graphite, GM2, and hydroxy-graphene (h-GO), respectively

pristine phases of α-MnO₂ and h-GO samples, respectively, with slight shift in positions with relative intensity variations, provided in Figs. SI-1a–b in the supporting information file. New peaks suggest formation of new planes in the composite which are absent in individual components. Such observations are distinct in GM2 rather than GM1 or GM3, asserting true composite formation in GM2.

To further ascertain the above fact, studies of relative thermal stability of the samples were carried out using TGA. Figure 1b shows the TGA profiles of pristine

graphite, hGO, and GM2 samples, respectively. The thermal instability of GM2 compared to pristine graphite is attributed to functionalization due to composite formation. Sample hGO has lower thermal stability and its decomposition is similar to functionalized graphenes available in the literature [37, 38]. However, for GM2, there is an initial weight loss (23%) around 250 °C which may be attributed to loss of adsorbed water as well as oxygen functionalities from the composite, but around 500 °C, the thermal stability increases by minimizing the provision for loss of carbon atoms from layer surfaces (as observed in hGO) due to anchoring of MnO_2 [15]. TGA profiles of GM1 and GM3 samples are provided in Figs. SI-2 in the supporting information. The profile of GM3 exhibits similar signature as that of hGO while the GM1 profile shows resemblance with pristine MnO_2 in accordance with previous rationalizations. Thus, the above study also substantiates the formation of the desired composite in GM2 sample.

The as-synthesized samples were subjected to morphological studies. Figure 2a, b displays the FESEM images of the sample GM2, showing uniform distribution of MnO_2 nanosheets anchored on h-GO sheet surfaces; Fig. 1b is the magnified part of encircled area of Fig. 2a. Figure 2c represents TEM image of the GM2 composite. Figure 2d, high-resolution transmission electron microscopy (HRTEM) of encircled area of image-2C, indicates lattice spacing of 2.42 (211) and 2.93 Å (310) are well in agreement for α-MnO_2 phase (JCPDS 44-0141), [35] and 3.14Å for hydroxy-functionalized graphene in the composite [34, 37, 38]. Morphological studies of GM1 and GM3 samples are shown in Supporting Information files: Figs. SI-3–SI-6, respectively. Due to the presence of excess Mn(II) ions in GM1 sample, it shows overgrowth of MnO_2 nanoparticles leading to the formation of MnO_2 nanoflowers deposited over h-GO sheets (as revealed from TEM image in SI-1, also supported by EDX studies (Fig. SI-9)). The above observation also supports why XRD and TGA results for GM1 sample mainly depict leading characteristic features of pristine MnO_2. On the other hand, in GM3 sample, due to small proportions of Mn(II) ions being employed, discrete as well as non-uniform distribution of MnO_2 nanoparticles results across the h-GO sheets.

It is worth mentioning that structures with porosity and interconnectivity provide additional accessible space for ions while maintaining sufficient conductivity for solid-state electronic transfer simultaneously. Such features are


Fig. 2 **a–d** SEM and TEM images of GM2 nanocomposite
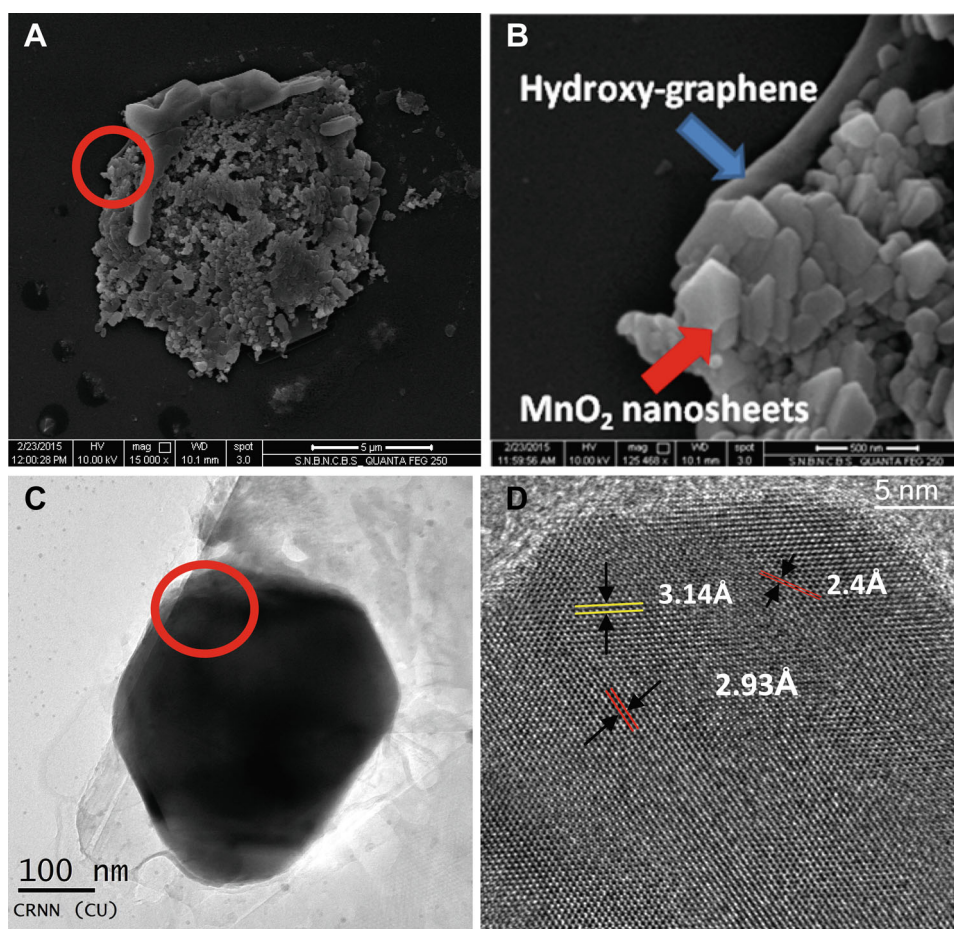
more prominent in GM2 sample. Additionally, we found that MnO_2 nanostructures remain strongly anchored on the surface of hGO sheets even after long exposure to ultra-sonication ($\sim$30 min) during sample preparation for TEM analyses, implying the existence of strong interaction between MnO_2 and hGO sheets which would enable fast electron transport through the underlying graphene layers resulting in the improvement of the electrochemical performance. Such proposition has also been confirmed by FTIR and Raman studies discussed below.

Both FTIR and Raman are very much complementary in investigating the nature of functionalities and degree of existing interactions between the components in the composite samples. FTIR analyses were carried out for GM1, GM2, GM3 and compared with that of the base material-hGO sample to understand the degree of functionality introduced. FTIR spectrum of GM2 sample, shown in Fig. 3a, depicts observed broad hump at 3500–3300 cm^{-1} indicating the presence of hydrogen bonded O–H groups [35]. Additionally, the broad peak centered around

Fig. 3 **a** FTIR of GM2 (*inset*: hGO sample). **b** Raman spectra of GM2 sample, graphite and hGO sample (*inset* shows the stretching peaks of MnO_2 in GM2 sample)
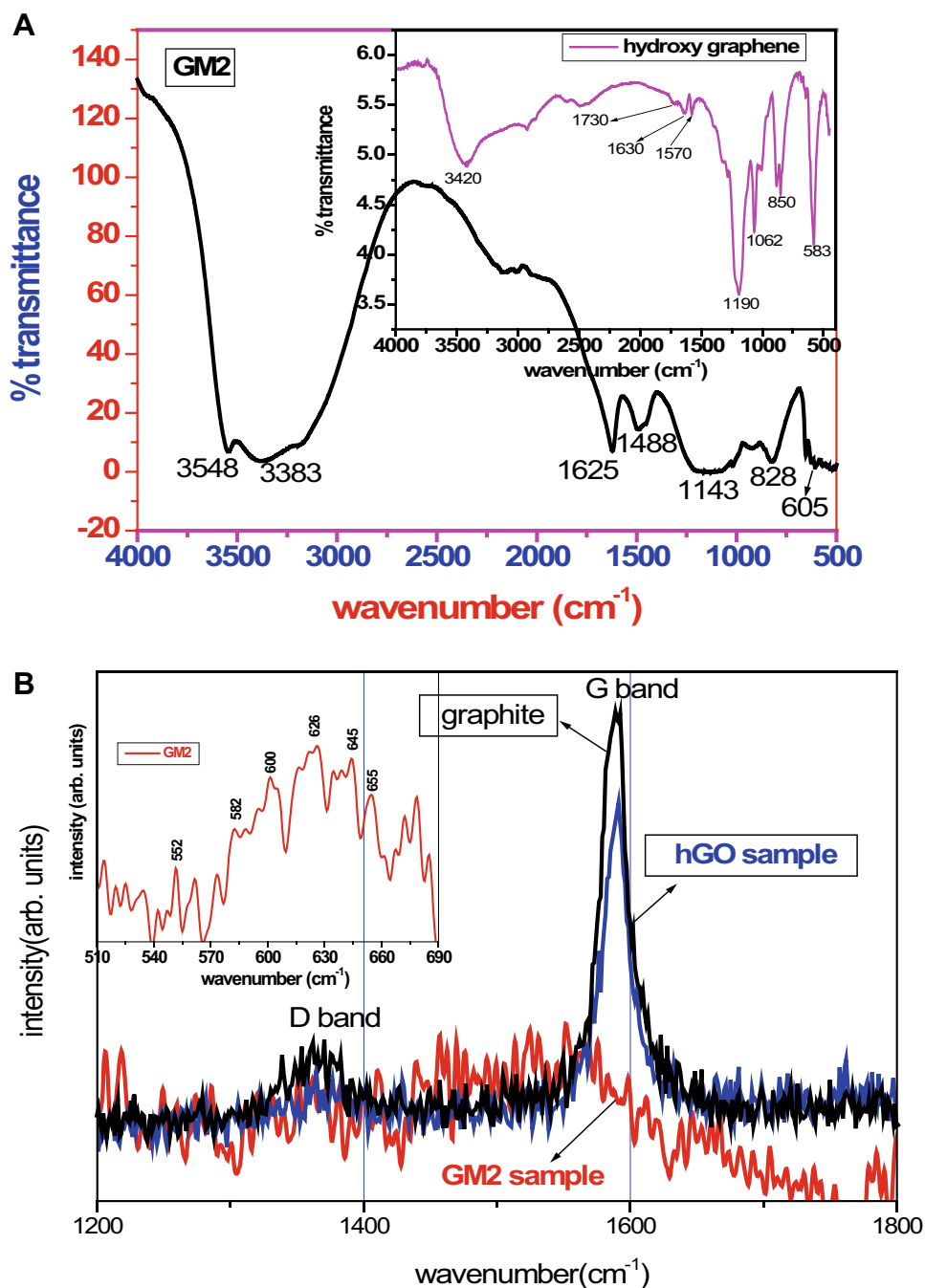
1143 cm^{-1} signifies the presence of C–OH group which confirms the presence of hydroxyl group in the graphene layers. Other peaks around 1550–1450 cm^{-1} (OH bending) and 1200–1100 cm^{-1} (C–O, C–C stretchings) are in accordance with earlier reports[35]. The shift of C=C stretching from 1630 to 1625 cm^{-1} clearly signifies the interaction with MnO$_2$ with graphene layers. Moreover, the existence of very feeble peak at 1720 cm^{-1} in GM2 asserts the presence of very little proportion of C=O of carbonyl and carboxylate functional groups in the material. So, we can conclude that the main oxygen-containing functional group is hydroxy (-OH) group in this case. We found that the relative peak intensity ratio of $\upsilon_{C=O}/\upsilon_{O-H}$ stretchings in pristine-GO (Supporting Information Fig. SI-7a) (0.88) is much higher than that in pristine hGO sample (inset of Fig. 3a) (0.56) which supports the formation of hydroxy-functionalized graphene in our case [38]. Furthermore, in GM2 composite, the peak at 605 cm^{-1} signifies the Mn–O-Mn vibrations, observed typically for MnO$_2$. Hence, the above analysis affirms the formation of hydroxyl-functionalized graphene/MnO$_2$ composite (GM2) [35, 36]. FTIR spectra of GM1 and GM3 samples are provided in Figs. SI-7b in the supporting information. The peaks in GM1 show prominent peaks for MnO$_2$ which GM3 shows spectral signature resembling hGO sample. It also appears that graphene sheets in GM3 are more O-functionalized than GM1, attributed to greater proportion of peroxodisulfate ion oxidizing graphite due to low concentration of Mn(II) species in former case, also supported by EDX studies as observed from Figs. SI-9. Thus, the formation of composite in its true sense is more prominent in GM2.

The extent of disorderness induced on composite formation in GM2 was explored by studying Raman spectroscopy of the samples (Fig. 3b). The Raman spectrum of graphite shows main peak at 1580 cm^{-1} (G-band) with a very weak peak at 1359 cm^{-1} (D-band), pertaining to less disorderness in the sp^2-C sheets [39, 40]. In hGO sample, the relative ratio of D/G bands increases due to increased sp^3-C domains on oxidation of graphite indicating disruption, modification, and defect formation in individual graphite layers. But the ratio is much lower than that reported in the case of graphene oxide, suggesting that the extent of oxidation is comparatively less in this case [41, 42]. Thus, creation of optimum defects due to O-functionalized graphene in hGO sample is hereby clearly indicated. In GM2, the ratio further increases along with peak-broadening attributed to higher disorderness. However, relative intensities of both peaks are drastically reduced which is caused due to strong anchoring of MnO$_2$ nanosheets onto hGO surfaces. It is again supported by the presence of several new peaks for Mn–O bond stretchings (inset graph of Fig. 3b) in the range 500–700 cm^{-1} well in agreement with literature [41, 42]. Accordingly, the above study suggests successful

integration of MnO$_2$ and hGO in the GM2 composite which is essential to obtain superior electrochemical performances.

3.1 Plausible mechanism of formation of GM composites

When graphite is sonicated with ammonium peroxodisulfate, the large peroxodisulfate ions intercalate and oxidize the graphite layers to form hydroxy-functionalized graphene (hGO) [34]. The aid of ultrasound energy helps in exfoliation of graphite layers and imparting necessary activation energy for electron-transfer to form hGO. Since the rate of oxidation is slower compared to other conventional oxidants, the specificity of the oxidation reaction is high and over-oxidation is restricted; thus, hydroxylation is effectively achieved.

$$S_2O_8^{2-} + 2H_2O \rightarrow 2SO_4^{2-} + 2H^+ + 1/2\ O_2$$

When Mn^{2+} ions are added, they get anchored on the defects (oxygen of hydroxy-groups) through electrostatic interactions on the layers of hGO sheets. These actually form the nucleation sites for MnO$_2$ nanoparticles formed from oxidation of Mn(II) ions by peroxodisulfate ions:

$$Mn^{2+} + S_2O_8^{2-} + 2H_2O \rightarrow MnO_2 + 2\ H_2SO_4$$
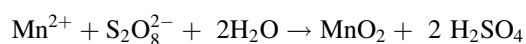
The growth process, as revealed from TEM image in Fig. 4a, starts from the formation of initially generated nuclei of MnO$_2$ nanoparticles on these h-GO sheets, particularly, when lower concentration of Mn(II) species is used during synthesis. It is well established that layered structures of Mn(IV) oxide are formed initially which then curl to transform to various shapes in order to minimize the surface energy [43, 44]. Large concentrations of water molecules and ammonium ions act as templating agents that stabilize the layered structure of MnO$_2$ [45–48]. This is again supplemented by the presence of large concentration of 2D hGO sheets acting as template for sheet morphology simultaneously. Thus, in this case, 3D growth of MnO$_2$ nanoparticles is restricted unlike in other conventional synthesis. Therefore, in Ostwald ripening process, smaller particles dissolve while the bigger ones grow into sheet-like morphology on the hGO 2D template surface as revealed from the SEM image in Fig. 4b. Nanosheets crystallize and aggregate with each other through cohesive forces to yield the larger sheets, which in turn convert to uniform hexagonal α-MnO$_2$ nanoplates (more thermodynamically favored phase) by local heat treatment offered by the sonochemical energy [45]. High degree of crystallinity (SAED inset of a MnO$_2$ nanosheet shown in Fig. 4c) is obtained as a result of matching of lattice parameters of 2.1 Å (211) of α-MnO$_2$ with {110} direction of h-GO as shown in Fig. 4d. This matching of

Fig. 4 a TEM image showing the formation of MnO₂ nanoparticles on h-GO sheets on preparing sample with low concentration of Mn(II) species. **b** SEM images of the formation of MnO₂ larger nanosheets/plates from aggregation of MnO₂ nanosheets on h-GO sheets in the GM2 composite. **c** HRTEM of a MnO₂ nanosheet (*inset* showing SAED pattern of it). **d** Diagram representing of {110} plane of graphite in h-GO showing lattice spacing of 2.14 Å {110} direction matching with the (211) lattice spacing of α-MnO₂
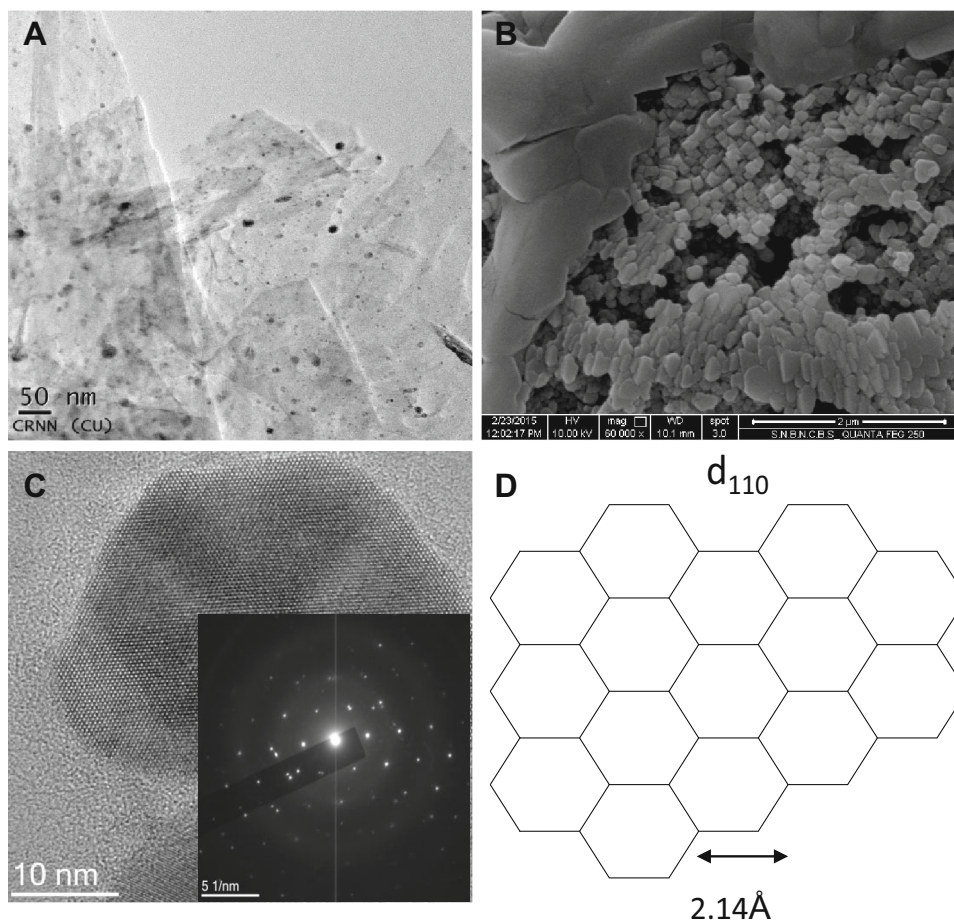
lattice parameters leads to epitaxial growth of MnO₂ nanosheets on h-GO substrate to form the GM2 composite. However, when large excess concentrations of Mn(II) ions are added, 3D growth of MnO₂ nanoparticles occurs resulting in the formation of nano-flowers as found in GM1 sample. Likewise, low concentration of Mn(II) ions leads to the formation of discrete inhomogeneous flakes of MnO₂ as observed for GM3 samples.

To explore the electrochemical behavior of both h-GO and GM2, cyclic voltammetry and galvanostatic charge/ discharge measurements were performed. Figure 5a shows the cyclic voltammograms (CVs) of GM2 composite at different scan rates respectively in the potential range −0.2 to +0.4 V versus saturated calomel electrode (SCE) in 1 M Na₂SO₄ medium. The CVs deviate from ideal rectangular shape due to double-layer capacitance as a result of contribution primarily originating from Faradic redox reactions from metal oxide to the capacitive behavior of the composite. The inset shows the CV of blank hydroxygraphene registered at 2 mVs⁻¹ scan rate. It reveals the Faradic nature in h-GO at negative potential (commencement of reduction of h-GO) which gets subdued through

composite formation. The specific capacitance (C_m) of these electrodes was calculated from the CV taken at the scan rate of 2 mVs⁻¹ according to the following equation [20, 49]:

$$C_m = i/mv,$$

where m is the mass of electro-active material; v is the potential sweep rate; and i is the even current response defined by (V_a and V_c represent the lowest and highest voltages, respectively) and obtained through integrating the area of the curves,

$$i = \int_{V_a}^{V_e} i(V)dV/(V_c - V_a).$$

The specific capacitance of GM2 composite was found to be 376.7 Fg⁻¹ at scan rate 2 mVs⁻¹. We also ran CVs at scan rate 2 mVs⁻¹ for both h-GO (CV plot shown in the inset of Fig. 5a) and blank MnO₂ samples (displayed in Fig. 5b), and the specific capacitances were found to be only 55.8 and 151.1 Fg⁻¹, respectively, reflecting synergistic effect of the individual components on specific capacitance in the composite. We have also carried out CV
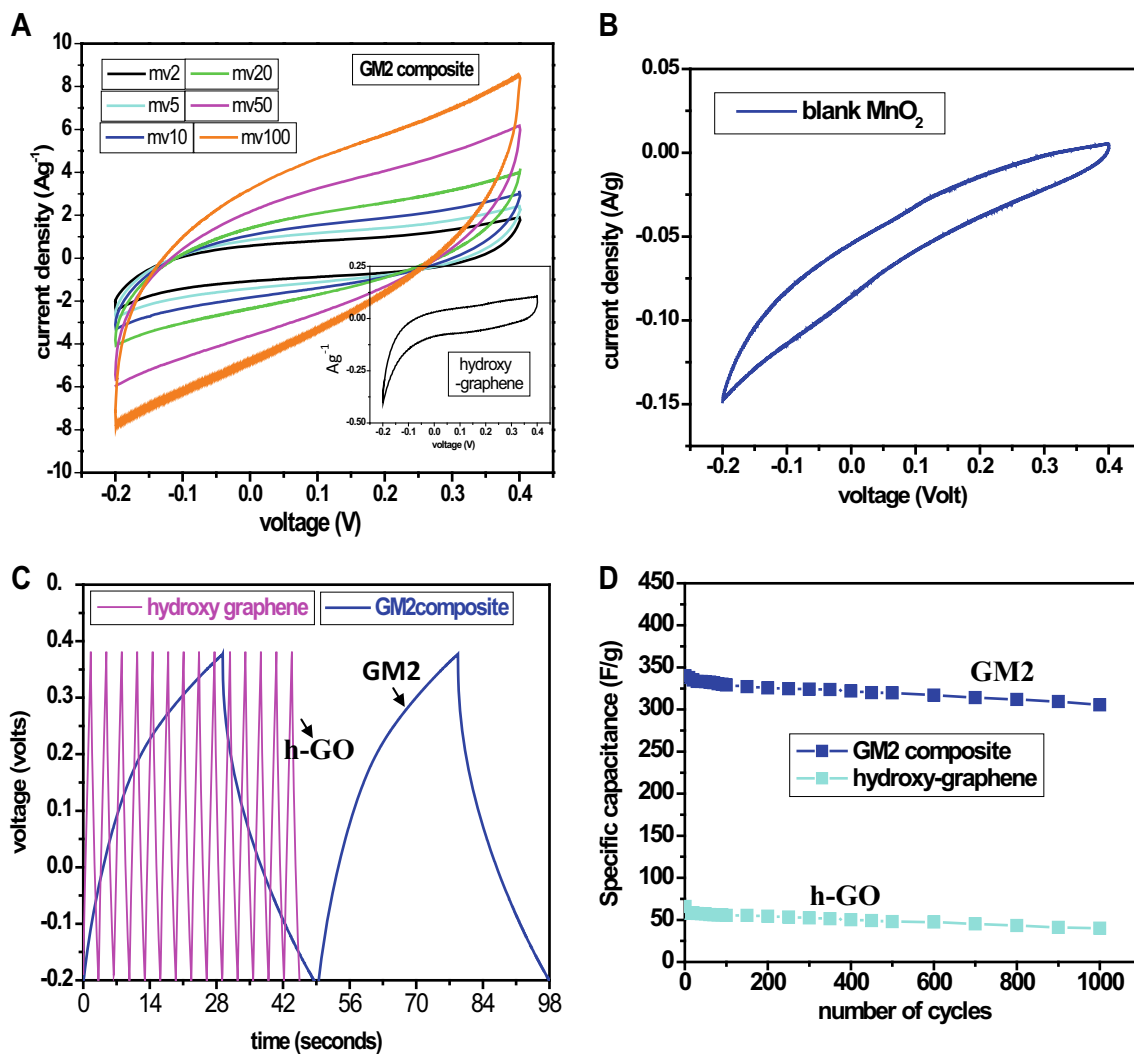
Fig. 5 **a** CVs of GM2 at different scan rates. *Inset* shows CV of hydroxy-graphene at 2 mVs^{-1} scan rate. **b** CV of blank MnO$_2$ at 2 mVs^{-1} scan rate. **c** Galvanostatic charging–discharging behavior at 7 A/g current density for both samples. **d** Cyclic performances of both the samples for charging/discharging profiles have been conducted for 1000 cycles at the current density of 7 A/g

for GM1 and GM3 samples, and the specific capacitances for the samples were 156.7 and 133.3 Fg^{-1}, respectively, at a scan rate of 2 mVs^{-1} under same measurement conditions shown in Fig. SI-8. The low specific capacitance in GM1 is attributed to poor conductivity of the thick MnO$_2$ layers. The capacitive behaviors of graphene sheets are thereby subdued in this case. On the other hand, very low, discrete and inhomogeneous distribution of MnO$_2$ nanoparticles on h-GO sheets in GM3 lowers its charge storing capacity. Thus, we can infer that GM2 has the higher specific capacitance among the synthesized composites.

Figure 5c shows the galvanostatic charging–discharging behavior for both the samples. The specific capacitance of the GM2 can be calculated from the GC curves using the following equation [20, 46]:

$$C_m = \frac{I\Delta t}{\Delta V m},$$

where I, Δt, ΔV, and m denote current density, discharge time, potential range in discharge after the IR drop, and the active mass of the material of the electrode, respectively. The specific capacitance values of the GM2 composite at current density of 7 Ag^{-1} are 333.3 Fg^{-1}, in accord with the results obtained from CV analysis. The value is appreciable in view with the aforesaid literature records.

The increase in supercapacitance in GM2 composites is mainly attributed to synergistic contribution from MnO$_2$ and h-GO components. The fact that hydroxy-functionalized graphene has better supercapacitive behavior owing to the presence of oxygen functionalities that help in trapping charges (EDLC) is supplemented by the presence of MnO$_2$

nanosheets which also on its own have intrinsic pseudo-capacitive behavior [50]. Pseudocapacitive materials can store much more energy than electric double-layer materials because the former undergo fast and reversible redox reactions at the electrode surface, besides conventional electric double-layer charge storage. Thus, sheet nature of MnO_2 anchored on hydroxy-functionalized graphene provides larger surface area for increasing the supercapacitive nature of the composite synergistically. We have also carried out BET surface area analyses which show that GM2 has approximately 1.36 times larger surface area compared to that of h-GO sample, which is consistent with the above proposition (displayed in Fig. SI-10).

In order to evaluate cycle performance of the samples, charge/discharge profiles have been conducted for 1000 cycles at the current density of 7 Ag^{-1}, and the results are depicted in Fig. 5d. As is expected, the capacitive retention for GM2 sample was about 91% after 1000 cycles, indicating a good cycling ability compared to hydroxy-graphene exhibiting only about 60% under similar situation. Thus, anchoring the MnO_2 nanosheets on the surfaces of hydroxy-graphene(h-GO) resulted in the enhanced charge storing capacity of the material by avoiding layer agglomeration and therefore long charge/discharge cycling ability was obtained.

Electrochemical Impedance Spectroscopy analysis of GM2 sample was carried out to investigate the degree of electrical conductivity and charge transport features of the composite. A Nyquist plot or complex-plane plot presents the impedance behavior as a function of frequency is shown in Fig. 6a–b. In the complex-plane, the imaginary component, Z", is usually used to represent the capacitive parameter and the real component Z', the ohmic one. The data of two components are collected simultaneously under a certain frequency range (100 kHz–0.1 Hz in the present study). The theoretical Nyquist plot of a supercapacitor consists of three regions which are dependent on the frequencies. At very high frequency, the supercapacitor behaves like a pure resistor [51]. At low frequency, the imaginary part sharply increases and a vertical line is usually observed, indicating a pure capacitive behavior. In the middle frequency domain, the influence of the electrode porosity can be observed. When the frequency decreases, starting from the very high frequency, the signal penetrates deeper and deeper inside the porous structure of the electrode, then more and more electrode surface becomes available for ion adsorption. In Fig. 6a, the Nyquist plot of the GM2 sample tends to appear as straight line almost parallel to the ordinate at low-frequency region indicating capacitive behavior. It also shows a small arc in the high-frequency region (shown in the inset also). The semi-circle loop has been observed and reported by numerous authors in the literature [51, 52]. A very big loop indicates large inter-
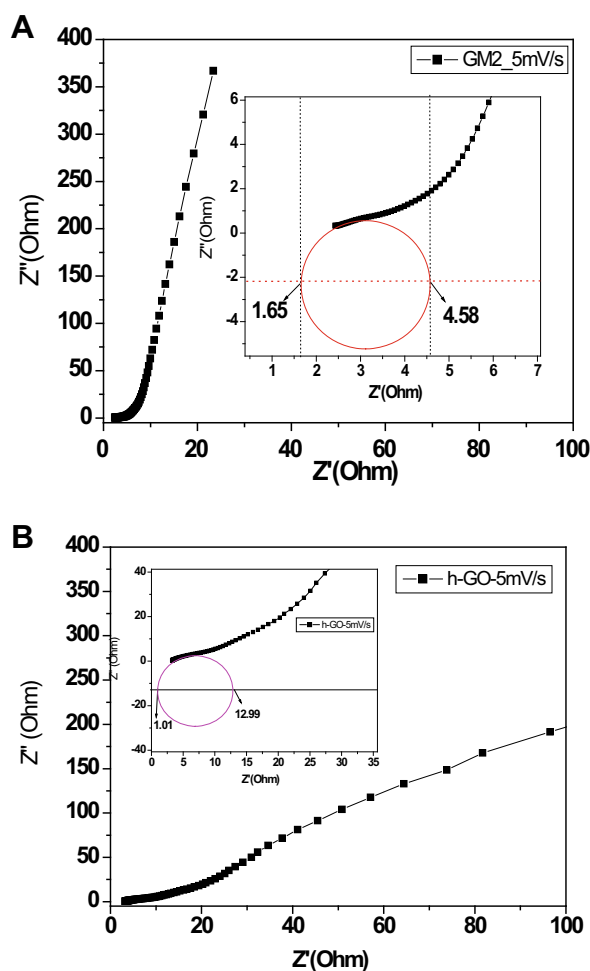

Fig. 6 a, **b** Nyquist plots for GM2 and h-GO sample-based electrodes at an amplitude of 5 mV versus Ag/AgCl over the frequency from 100 kHz to 0.1 Hz Z' is the real impedance and Z" is the imaginary impedance in ohms. Inset in each case showing the magnified portion of the graph in the high-frequency regime

granular electrical resistance between the particles. It largely depends on the electrode surface area and the inter-particle resistivity. The realization of thin active layers or adding some low surface area conductive additives can reduce this value. The obtained small loop regions in the present case show a low electrical resistance between the MnO_2-anchored functionalized graphene nanosheets and good conductivity between the composite electrode and current collector, attributing to the epitaxial growth of nanostructured MnO_2 on the h-GO sheets rather than a mechanical blending. We could also find in the Nyquist plot that GM2 has more straight line than the pure h-GO electrode (displayed in Fig. 6b) in the low-frequency region. The growth of the MnO_2 nanostructures could therefore broaden the distance between the graphene nanosheets, which would then to make it easier for electrolyte ion transfer. From the Nyquist plot of GM2, the equivalent series resistance (ESR) is calculated to be around $\sim 2.38\ \Omega$

and charge transfer resistance (R_{CT}) of ~ 2.93 Ω, respectively, compared to h-GO sample showing ESR of 3.01Ω and R_{CT} of 11.98Ω; the small resistance value in the composite thus supports our earlier rationalizations [51, 52].

4 Conclusion

MnO_2 nanosheet-anchored hydroxy-functionalized graphene has been successfully synthesized by a simple one-pot, green and wet-chemical method with the aid of ultrasonic energy. A plausible mechanism for the formation of the nanocomposite has been proposed. The studies reveal that GM2 possesses the optimum structural and electronic features as dictated by composition of C:Mn ratio, to obtain the highest charge storing capacity among the samples studied. The sheet-like morphology is supposed to provide two additional advantages, namely (a) better diffusion path lengths both for ions and electrons and (b) sufficient porosity for electrolyte penetration promoting high charging and discharging rates. Thus, the electrode constructed with the with GM2 sample exhibited better electrical conductivity and ion transport performances pertaining to appreciable specific capacitance, stable cycling performance for supercapacitor applications. Considering the low cost, abundant resources, simplicity of the preparative method and improved electrochemical properties, we believe that the composite can be considered as promising electrode material for energy storage devices.

References

1. Burke A (2000) Ultracapacitors: why, how, and where is the technology. J Power Sources 91(1):37–50
2. Winter M, Brodd RJ (2004) What are batteries, fuel cells, and supercapacitors? Chem Rev 104(10):4245–4270
3. Mahmood N, Zhang C, Yin H, Hou Y (2014) Graphene-based nanocomposites for energy storage and conversion in lithium batteries, supercapacitors and fuel cells. J Mater Chem A 2:15–32
4. El-Kady MF, Strong V, Dubin S, Kaner RB (2012) Laser scribing of high-performance and flexible graphene-based electrochemical capacitors. Science 335:1326–1330
5. Chen S, Zhu J, Wu X, Han Q, Wang X (2010) Graphene oxide—MnO_2 nano composites for supercapacitors. ACS Nano 4(5):2822–2830
6. Ge J, Yao HB, Hu W, Yu XF, Yan YX, Mao LB, Li HH, Li SS, Yu SH (2013) Facile dip coating processed graphene/MnO_2-nanostructured sponges as high performance supercapacitor electrodes. Nano Energy 2(4):505–513
7. Subramanian V, Zhu HW, Vajtai R, Ajayan PM, Wei BQ (2005) Hydrothermal synthesis and pseudocapacitance properties of MnO_2 nanostructures. J Phys Chem B 109(43):20207–20214
8. Majumdar D, Baugh N, Bhattacharya SK (2017) Ultrasound assisted formation of reduced graphene oxide-copper(II) oxide nanocomposite for energy storage applications. Colloids Surf A 512:158–170
9. Peng L, Peng X, Liu B, Wu C, Xie Y, Yu G (2013) Ultrathin two-dimensional MnO_2/graphene hybrid nanostructures for high-performance, flexible planar supercapacitors. Nano Lett. 13(5):2151–2157
10. Yan J, Fan ZJ, Wei T, Qian WZ, Zhang ML, Wei F (2010) Fast and reversible surface redox reaction of graphene-MnO_2 composites as supercapacitor electrodes. Carbon 48(13):3825–3833
11. Cheng Q, Tang J, Ma J, Zhang H, Shinya N, Qin LC (2010) Graphene and nanostructured MnO_2 composite electrodes for supercapacitors. Carbon 49:2917–2925
12. Li Z, Mi Y, Liu X, Liu S, Yang S, Wang J (2011) Flexible graphene/MnO_2 composite papers for supercapacitor electrodes. J Mater Chem 21:14706–14711
13. Dimiev AM, Bachilo SM, Saito R, Tour JM (2012) Reversible formation of ammonium persulfate/sulfuric acid graphite intercalation compounds and their peculiar Raman spectra. ACS Nano 6(9):7842–7849
14. Wu L, Zhang B, Lu H, Liu CY (2014) Nanoscale ionic materials based on hydroxyl-functionalized graphene. J Mater Chem A 2:1409–1417
15. Feng X, Zhang Y, Song J, Chen N, Zhou J, Huang Z, Ma Y, Zhang L, Wang L (2015) MnO_2/graphene nanocomposites for nonenzymatic electrochemical detection of hydrogen peroxide. Electroanalysis 27(2):353–359
16. Sung DY, Gunjakar JL, Kim TW, Kim IY, Lee YR, Hwang SJ (2013) Graphene-assisted room-temperature synthesis of 2D nanostructured hybrid electrode materials: dramatic acceleration of the formation rate of 2D metal oxide nanoplates induced by reduced graphene oxide nanosheets. Chem—Eur J 19:7109
17. Moazami HR, Davarani SSH, Yousefi T, Keshtkar AR (2015) Synthesis of manganese dioxide nanosheets and charge storage evaluation. Mater Sci Semicond Process 30:682–687
18. Sinha AK, Pradhan M, Pal T (2013) Morphological evolution of two-dimensional MnO_2 nanosheets and their shape transformation to one-dimensional ultralong MnO_2 nanowires for robust catalytic activity. J Phys Chem C 117:23976–23986
19. Fan Z, Yan J, Wei T, Zhi L, Ning G, Li T, Wei F (2011) Asymmetric supercapacitors based on graphene/MnO_2 and activated carbon nanofiber electrodes with high power and energy density. Adv Funct Mater 21:2366–2375
20. Qian Y, Lu S, Gao F (2011) Preparation of MnO_2/graphene composite as electrode material for supercapacitors. J Mater Sci 46(10):3517–3522
21. Yang H, Jiang J, Zhou W, Lai L, Xi L, Lam YM, Shen Z, Khezri B, Yu T (2011) Influences of graphene oxide support on the electrochemical performances of graphene oxide-MnO_2 nanocomposites. Nanoscale Res Lett 6(1–8):531
22. Li Z, Wang J, Liu S, Liu X, Yang S (2011) Synthesis of hydrothermally reduced graphene/MnO_2 composites and their electrochemical properties as supercapacitors. J Power Sources 196(19):8160–8165
23. Zhu C, Guo S, Fang Y, Han L, Wang E, Dong S (2011) One-step electrochemical approach to the synthesis of Graphene/MnO_2 nanowall hybrids. Nano Res 4(7):648–657

24. George AT, Ganesan R, Thangeeswari T (2016) Redox deposition of manganese oxide nanoparticles on graphite electrode by immersion technique for electrochemical super capacitors. Ind J Sci Technol 9(1):1–7

25. Wu Z-S, Ren W, Wang D-W, Li F, Liu B, Cheng H-M (2010) High-energy MnO_2 nanowire/graphene and graphene asymmetric electrochemical capacitors. ACS Nano 4(10):5835–5842

26. Zhu J, He J (2012) Facile synthesis of graphene-wrapped honeycomb MnO_2 nanospheres and their application in supercapacitors. ACS Appl Mater Interfaces 4(3):1770–1776

27. Jafta CJ, Rouxa FNL, Mathea MK, Kebedea M, Makgopa K, Song Y, Tong D, Oyama M, Manyala N, Chend S, Ozoemena KI (2013) Manganese oxide/graphene oxide composites for high-energy aqueous asymmetric electrochemical capacitors. Electrochim Acta 110:228–233

28. Kim M, Hwang Y, Min K, Kim J (2013) Concentration dependence of graphene oxide–nanoneedle manganese oxide composites reduced by hydrazine hydrate for an electrochemical supercapacitor. Phys Chem Chem Phys 15:15602–15611

29. Yu G, Hu L, Vosgueritchian M, Wang H, Xie X, McDonough JR, Cui X, Cui Y, Bao Z (2011) Solution-processed graphene/MnO_2 nanostructured textiles for high-performance electrochemical capacitors. Nano Lett 11:2905–2911

30. He Y, Chen W, Li X, Zhang Z, Fu J, Zhao C, Xie E (2013) Freestanding three-dimensional graphene/MnO_2 composite networks as ultralight and flexible supercapacitor electrodes. ACS Nano 7(1):174–182

31. Lee H, Kang J, Cho MS, Choi J-B, Lee Y (2011) MnO_2/graphene composite electrodes for supercapacitors: the effect of graphene intercalation on capacitance. J Mater Chem 21:18215–18219

32. Kim M, Yoo M, Yoo Y, Kim J (2014) Capacitance behavior of composites for supercapacitor applications prepared with different durations of graphene/nanoneedle MnO_2 reduction. Microelectron Reliab 54:587–594

33. Jin Y, Chen H, Chen M, Liu N, Li Q (2013) Graphene-patched CNT/MnO_2 nanocomposite papers for the electrode of high-performance flexible asymmetric supercapacitors. ACS Appl Mater Interfaces 5:3408–3416

34. Majumdar D, Pal S (2016) Hydroxy-functionalized graphene: a proficient energy storage material. J Fundam Renew Energy Appl 6(1–4):209

35. Zhang YX, Zhu S, Dong M, Liu CP, Wen ZQ (2013) Hydrothermally tailoring low-dimensional MnO_x nanostructure and their high electrochemical performance. Int J Electrochem Sci 8:2407–2416

36. Chu H-A, Sackett H, Babcock GT (2000) Identification of a Mn-O-Mn cluster vibrational mode of the oxygen-evolving complex in photosystem II by low-frequency FTIR spectroscopy. Biochemistry 39(47):14371–14376

37. Zhao Y, Misch J, Wang C-A (2016) Facile synthesis and characterization of MnO_2 nanomaterials as supercapacitor electrode materials. J Mater Sci 27(6):5533–5542

38. Feng X, Yan Z, Chen N, Zhang Y, Ma Y, Liu X, Fan Q, Wang L, Huang W (2013) The synthesis of shape-controlled MnO_2/graphene composites via a facile one-step hydrothermal method and their application in supercapacitors. J Mater Chem A 1:12818–12825

39. Liu W-W, Chai S-P, Mohamed AR, Hashim U (2014) Synthesis and characterization of graphene and carbon nanotubes: a review on the past and recent developments. J Ind Eng Chem 20:1171–1185

40. Kudin KN, Ozbas B, Schniepp H C, Prud'homme RK, Aksay IA, Car R (2008) Raman spectra of graphite oxide and functionalized graphene sheets. Nano Lett 8(1):36–41

41. Hsu Y-K, Chen Y-C, Lin Y-G, Chen L-C, Chen K-H (2011) Reversible phase transformation of MnO2 nanosheets in an electrochemical capacitor investigated by in situ Raman spectroscopy. Chem Commun 47:1252–1254

42. Li J, Ren Z, Wang S, Ren Y, Qiu Y, Yu J (2016) MnO_2 nanosheets grown on internal surface of macroporous carbon with enhanced electrochemical performance for supercapacitors. ACS Sustain Chem Eng 4:3641–3648

43. Wang X, Li YD (2003) Synthesis and formation mechanism of manganese dioxide nanowires/nanorods. Chem Eur J 9:300–306

44. Huang M, Li F, Dong F, Zhang YX, Zhang LL (2015) MnO_2-based nanostructures for high-performance supercapacitors. J Mater Chem A 3:21380–21423

45. Suslick KS (1990) Sonochemistry. Science 247:1439–1445

46. Meher SK, Rao GR (2013) Enhanced activity of microwave synthesized hierarchical MnO$_2$ for high performance supercapacitor applications. J Phys Chem C 117(10):4888–4900

47. Xiao W, Wang D, Lou XW (2010) Shape-controlled synthesis of MnO_2 nanostructures with enhanced electrocatalytic activity for oxygen reduction. J Phys Chem C 114(3):1694–1700

48. Pang SC, Chin SF, Ling CY (2012) Controlled synthesis of manganese dioxide nanostructures via a facile hydrothermal route. J Nanomater. doi:10.1155/2012/607870

49. Fan Z, Yan J, Wei T, Zhi L, Ning G, Li T, Wei F (2011) Asymmetric supercapacitors based on graphene/MnO_2 and activated carbon nanofiber electrodes with high power and energy density. Adv Funct Mater 21:2366–2375

50. Lee M-T, Tsai W-T, Deng M-J, Cheng H-F, Sun I-W, Chang J (2010) Pseudocapacitance of MnO_2 originates from reversible insertion/desertion of thiocyanate anions studied using in situ X-ray absorption spectroscopy in ionic liquid electrolyte. J Power Sources 195:919–922

51. Hassan S, Suzuki M, El-Moneim AA (2014) Facile synthesis of MnO_2/graphene electrode by two-steps electrodeposition for energy storage application. Int J Electrochem Sci 9:8340–8354

52. Gao H, Xiao F, Ching CB, Duan H (2012) High-performance asymmetric supercapacitor based on graphene hydrogel and nanostructured MnO_2. ACS Appl Mater Interfaces 4(5):2801–2810